Scientific Research Publishing

Engineering, 2025, 17(12), 635-658
https://www.scirp.org/journal/eng
ISSN Online: 1947-394X
ISSN Print: 1947-3931

Experimental Investigations of Chemical Flooding Using Air Injection Boosters for Improved Oil Recovery in Mature Reservoirs (Brownfields)

Fahad Rashid*, Godpower Enyi

Petroleum and Gas Engineering Division, School of Science, Engineering, and Environment, University of Salford, Manchester, UK
Email: *f.m.s.rashia@edu.salford.ac.uk

How to cite this paper: Rashid, F. and Enyi, G. (2025) Experimental Investigations of Chemical Flooding Using Air Injection Boosters for Improved Oil Recovery in Mature Reservoirs (Brownfields). *Engineering*, **17**, 635-658.
https://doi.org/10.4236/eng.2025.1712036

Received: October 17, 2025
Accepted: December 20, 2025
Published: December 23, 2025

Abstract

To recover oil from brownfields, test air booster chemical flooding. Silica nanoparticle-polymer Arabic gum (SP) solution injection with controlled air injection is studied for displacement efficiency synergy. Multiple crude oil-soaked core samples were employed in lab core flooding procedures to approximate reservoir conditions. Performance depended on pressure drop, burst duration, and oil recovery. Study: continuous oxygen air flooding eliminates less oil from the ground than AAW. Results from experiments supported this. Air alternative water (AAW) optimises oil recovery and efficiency by regulating flow. In congested reservoirs, air can replace water. Constant air sealing keeps oil from water. Air alternative water (AAW) systems use polymers like Arabic gum, silica nanoparticles, and a mix of the two to remove oil and prevent water contamination. Nano-polymer-alternating-water (NPAW) creates air alternate water (AAW). Three-phase flow with silica and Arabic gum is studied in this study. A two-phase investigation used combination, silica, and polymer/oil. Water/oil and combination/oil displacement boosted oil output and relative permeability, unlike polymer/oil and nanoparticles. Air and oil have lower surface resistance than water. Air injection sweeps outperform water floods technically. Lab scientists analyse chemical fluid-oil interfacial tension with polymer-silica and NaCl. Air, fluid, and fluid injections recovered 48.6%, 20%, and 16.7% of oil in core flooding testing. This reveals that air, Arabic gum, and silica nanoparticles greatly improve lab core oil recovery. The air boosters increased oil flow, residual saturation, and sweep. Chemicals and air injection improve older deposit EOR.

Keywords

EOR, Air Injection, Chemical Flooding, Silica Nanoparticles, Polymer Flooding, Arabic Gum, Air-Alternate-Water (AAW), NPAW, Core Flooding, Mature Reservoirs, Brownfields, Oil Displacement Efficiency

1. Introduction

Energy demand is rising as primary, or natural recovery methods, deplete hydrocarbon sources worldwide. Figure 1 demonstrates that the main recovery begins initially. It uses the reservoir's natural energy to recover 5% - 10% of the original oil in situ (OOIP). Oil recovery declines significantly when natural energy is scarce due to secondary recovery. This requires a new energy source in the natural energy system. Simple water flooding and non-miscible gas injection are the basic secondary recovery strategies. They can recover 20% - 30% of the oil in situ. Tertiary or enhanced oil recovery (EOR) procedures are used when these fail. Flooding with polymers, alkali, surfactants, and nanoparticles. EOR methods remove residual oil and increase OOIP recovery to 70%.

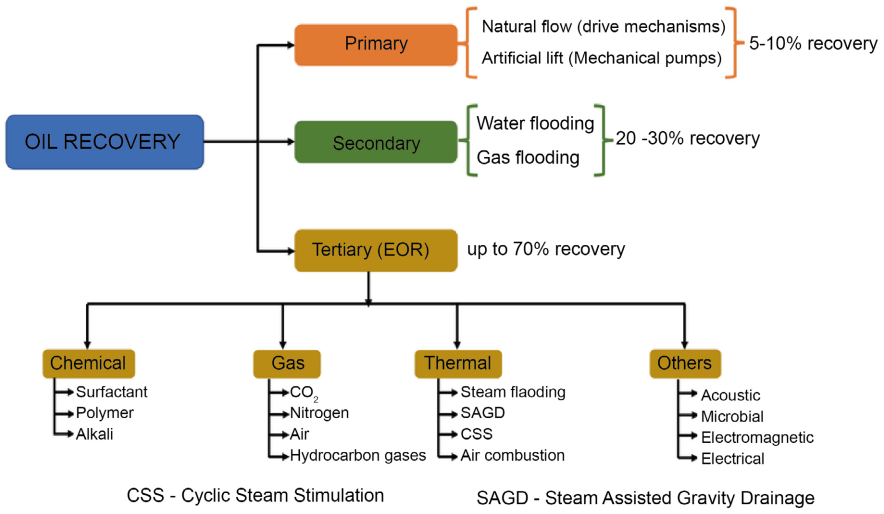

Figure 1. Categories of oil recovery.

Hydrolysed polyacrylamides and xanthan gums dominate oil field applications. As of now, no oil field applications have used nanoparticles and Arabic gum polymer. Water dissolves hydrolysed polyacrylamides from recent months. According to [1], Arabic gums, a polymer, thicken liquids well. Research confirms this. These polymers don't fulfil criteria even though they're used. Careful recovery can recover 15% - 30% of the oil initially installed. Nanotechnology defines a particle as a small entity that behaves based on its attributes and movement. This phrase implies particle movement. They have been studied for usage in polymer composites, solar cells [2] and [3], and medication delivery [4]. Researchers examined

various applications for potential benefits. These are some of the many uses studied. They affect surface properties because they are surface active. To use nanoparticles efficiently, we need reflections beyond their interfacial properties. The main reason is that these methods may improve oil recovery [5]. This is the main cause. [6] suggests using nanoparticles to solve oil industry recovery issues. This group includes adsorption and chemical thermal degradation. A reservoir and fluid-specific solution is always utilised to inject nanoparticles into a formation at field size. This ensures proper formation. This cannot be disputed, regardless of the situation. Polymer thickens water. Thus, a thick, stable solution is preferred. This is because polymers thicken water. The mobility ratio has decreased due to this adjustment, causing this behaviour. This project plans to distribute heavy oil with nanoparticles. Scientists have studied nanoparticles for oil recovery (EOR). Much research has examined this [5]. However, nanoparticles are growing swiftly and may recover more oil than nanoparticles. Nanomaterials are becoming more frequent. Polymer-coated nanoparticles are a fast-changing substance. Some term these nanoparticles "polymer-coated nanoparticles" because they have polymer chains on their surfaces. The phrase is used because of this. As said, this is due to greater stability, medium spreading, and foam and emulsion stabilisation. Another factor is how well it dissolves in fluids. Nano-fluids may solve these issues. This is because nanofluids thicken injected fluids. Two major technologies allow nanoparticle oil recovery. Use polymer- and surfactant-covered nanoparticles and wettability approaches to control mobility. Nanoparticle wedge films provide structural disjoining pressure that separates oil from rock surfaces [7]. These methods may improve healing and microscopic displacement. (**Figure 2**)

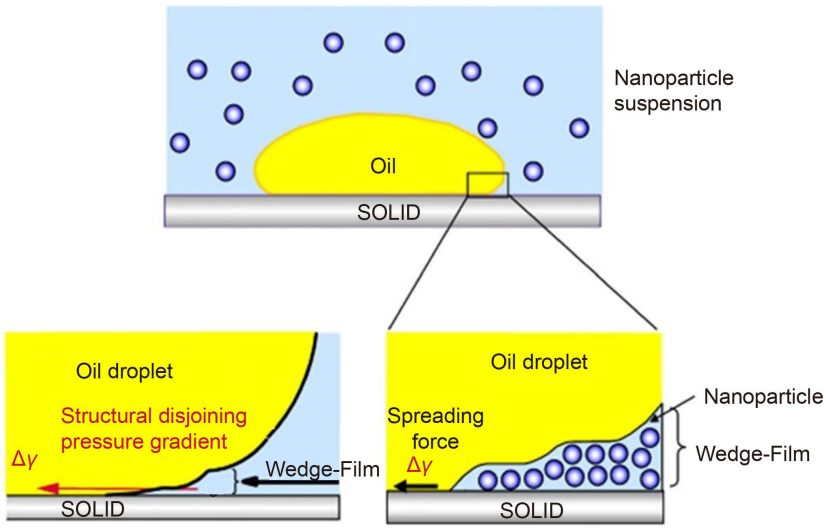

Figure 2. Structural disjoining pressure.

The Amott test, contact angle measurements, and core displacement tests are common laboratory wettability tests [8] and [9]. This study evaluates nanoparticle polymer systems in reservoir conditions using core flooding experiments. Nano-

particles are cheaper than specialty compounds, thus they can be used in Enhanced Oil Recovery when prices drop. Since nanoparticles are less hazardous and environmentally friendly than conventional chemical procedures, they can be used widely [10]. The idea is to mix silica nanoparticles and Arabic gum polymer with air to propel them. This blended technique will be tested for recovery in homogeneous and heterogeneous reservoirs. The experiment carefully assesses oil displacement across various core samples, Nano polymer fluid injection following water flooding, and recovery performance. Flue gas sweep is also caused by crude oil oxidation in the environment. An EOR approach that lowers IFT involves crude oil and ground air. The contact may also reduce IFT. China's typical air injection method may have been replaced with low-oxygen air injection in recent years. This reduces pipeline corrosion and risk. Most oil fields worldwide develop via water flooding after the first step of reduction. Because of this, the current oil field often enters a high water cut production phase, making extension and crude oil recovery tougher. Water cuts will be increased to achieve this. For reservoir development, engineers prefer polymer floods or nanoparticles for tertiary oil recovery because these two tactics are more likely to work. Because their acceptance is more likely to succeed. These technologies have great potential but are expensive and require reservoir parameters like salinity and temperature. This study tests silica nanoparticles, air injection, and Arabic gum polymer in mature reservoirs with different salinities.

2. Materials and Equipment for Experiments

2.1. Sample Preparation and Measurement

We measured core samples' diameter, length, weight, and petrophysical parameters (porosity and permeability). To reduce errors, each sample was measured three times and the average was used in computations. After drying in a 90˚C oven for 24 hours, the samples were weighed again to ensure stability. After cooling, the samples were returned to the oven to maintain dry weight. The following porosity and saturation estimates were accurate after these processes.

2.2. Porosity

All pore space moisture will evaporate after the core sample is thoroughly dry. When the sample is saturated with water, all connecting pore spaces are presumed to be full. Weighing the difference in weight shows how much water is in the pores. You can calculate water volume using a simple formula if you know its density. Using prior geometric data, you may simply calculate the core's bulk volume. This porosity is called "effective porosity". The effective pore volume, which determines porosity, is the space between pores. The same procedure was used to evaluate porosity on all core samples. They were oven-dried for 24 hours before soaking in water for 24 hours.

$$\varnothing = \frac{\mathrm{PV}}{\mathrm{BV}} \times 100 \tag{1}$$

where:

$\varnothing$ = Porosity

PV = Pore volume

BV = Bulk volume

2.3. Permeability

The most basic test is absolute permeability. To measure absolute permeability, single-phase fluids were fed into the core at varying flow rates and pressures were dropped. Permeability numbers were calculated using Darcy's law. Tests were done at 500 psi and ambient temperature. The flow rates (1 - 2.5 ml/min) were tried until pressure stabilised. The pressures were recorded using SmartFlood. This approach accurately evaluated core permeability, which is crucial for understanding flood fluid movement. Check out this Darcy equation:

$$k = \frac{Q\mu L}{A\Delta P} \tag{2}$$

where:

k Permeability (md)

Q Flowrate (ml/m)

μ Viscosity (cp)

A Area (cm^2)

L Length (cm)

ΔP Differential pressure (ΔP)

3. Materials and Methods

3.1. Core Samples

A variety of materials were used for project analysis. Core samples, crude oil with an API of 32, silicon nanoparticles, gum Arabic, brine, and air are in this collection. Air is also in this set. Set includes an air source. Several core specimens and their properties are shown below. This experiment used core samples from the Sandston family. The samples came from Kocurek Industries Inc. These findings match data in Table 1.

Table 1. Different types of core samples.

	Core name	Homogeneous	Formation
	Bernheimer	Yes	Valaginian
	Michigan	Yes	Paleozoic

Continued

	Nugget	No	Late Triassic
	Salt Wash North	Yes	Late Cretaceous
	Leopard Sandstone	No	Paleozoic
	Castlegate	Yes	Late Cretaceous

3.2. Crude Oil

Kuwait's crude oil possesses an API gravity of 22 degrees, categorising it as medium crude. Table 2 provides a summary of the qualities of the crude oil.

Table 2. Characteristics of crude oil.

API	22
Viscosity	(cP) 9.7
Water Content	9.2
Density (g/cm^3)	0.871

3.3. Arabic Gum Polymer

Acacia Senegal, Sieberiana, and nilotica occur in woodlands near Batagawara Village in Katsina. These trees were used to harvest gum Arabic samples. From tree barks, samples were collected as dry nodules or lumps. Figure 3 shows the tree bark Arabic gum polymer type.

Figure 3. Arabic gum powder.

3.4. Silica Nanoparticles

Silica nanoparticles (SNPs) are the most common nanoparticles used in oil recovery (Figure 4). When examined, these nanoparticles contain 99.8% silicon dioxide, the primary component of sandstone. Brine-based silica nanofluid contains different concentrations of silica nano and brine. This solution was well mixed after several hours of magnetic stirring.

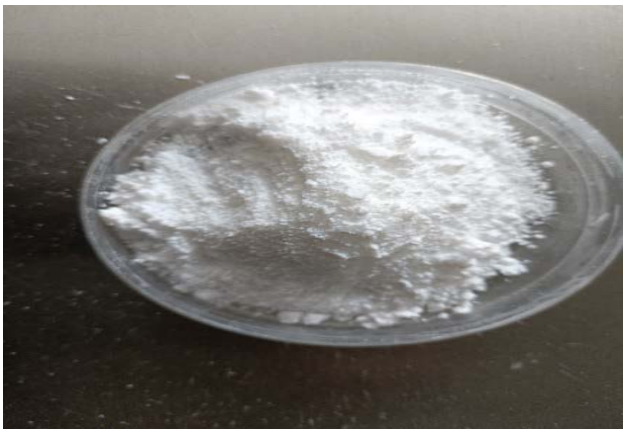

Figure 4. Particles of silica nanoparticles.

3.5. Brine Solutions

Different chloride salinities were tested for this investigation. These concentrations varied from 5% to 20% by weight. Concentrations were sorted by weight percentage. A precise balance lets us make the proper brine concentrations. Chloride solutions and distilled water were mixed in a round-bottom flask. A magnetic stirrer slowly spun the mixture for 24 hours. To dissolve the salts entirely. After the salts dissolved in the water, viscosities were tested and recorded (Figure 5).

Figure 5. Brine preparation.

4. The Experimental Method

Soxhlet Extractor

The Soxhlet Extractor is a tool that is used to get lipids out of solid materials. It is also often used in core analysis, where core samples are taken out to get rid of

water and oil as shown in Figure 6. This is because the Soxhlet Extractor takes both parts out of core samples.

Figure 6. Soxhlet extractor to clean the core samples.

Saturation of the External Core Sample

Before being saturated with oil, the core is dried and weighed. Following saturation, the sample is weighed again M_1, and the difference between the two weights determines the amount of oil in the pores M_2. Calculate the rock's pore space oil by converting the core sample's rise in grammes to millilitres. Knowing oil density allows this. This apparatus oils core samples for seven days before the experiment and air injection (Figure 7). This happens before the experiment.

M = The excess oil in the core sample in grams must be converted to millilitres.

M_2 = The core sample weight with oil saturation.

M_1 = The core sample weight after cleaning and drying.

After oil saturation, the core sample is put in the central container and kept at temperature and pressure for 24 hours. Within the context of the crude oil, brine, and rock system, this process, which is referred to as core ageing, tries to precisely reproduce the conditions that existed in the past.

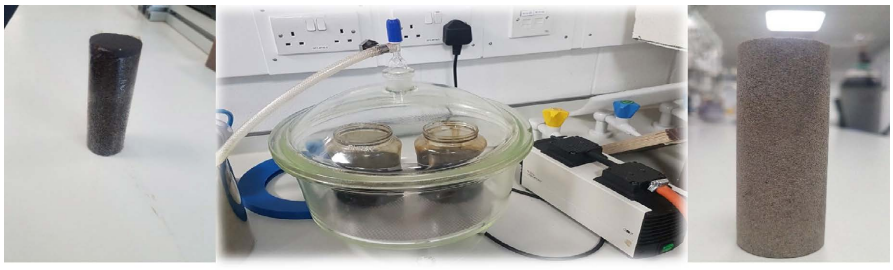

Figure 7. (A) A core sample after saturation; (B) Vacuum to achieve external oil saturation; (C) A core sample before saturation.

PREL-300 Core Laboratories

The Reservoir Permeability Tester measures core sample permeability. The pro-

ject's criteria may need gas injection or water flooding of these samples. The RPT also monitors and calculates oil and water saturations, water and residual oil saturations, oil recovery rates, and permeability variations. In addition, it can measure and calculate many data types. Air injection and polymer and nano-fluid flooding were used to test oil recovery. The remaining oil saturations and water and oil saturations were also measured. Figure 8 below provides RPT details.

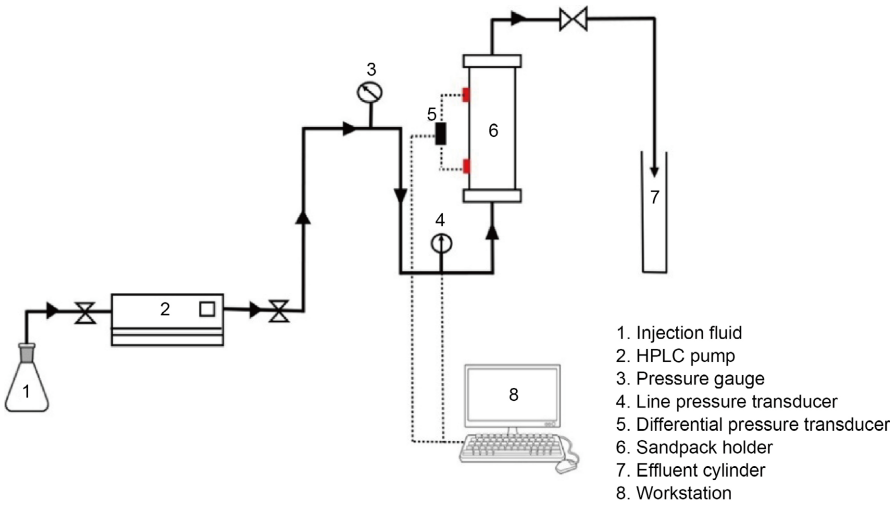

Figure 8. Overview of the core flooding diagram.

Procedure:

Two-Phase

Experiment with Nano Fluid (Silica Nanoparticles) and Oil

The following processes moved nanofluids and oil for experiment. Following washing and drying, the core was measured for length and width. These measurements are in the release report. The core's weight was weighed and recorded. The core sample was fully submerged in oil after 7 days. Reweighed to ascertain oil content. The sample's oil content was confirmed. The core sample was placed in the core holder after processing. 2,000 pounds per square inch confining pressure was applied to the core to imitate reservoir overburden. To maintain 1000 pounds per square inch, a back-pressure gauge was used. After obtaining the right temperature and pressure, fluid was infused and temperature adjusted for three days to mature the core. The procedure began after prerequisites were met. Nano fluid injection rates were 0.5 and 1 ml/min. Infusion was steady. Nano fluid was pushed till oil saturation was reached.

Three-Phase

Alternating Displacement Experiment with Air, Fluid, and Oil

Wash and dry the core, then measure its length and diameter with a calliper. Later, the core was scaled. The weighed sample enters the core holder after 7 days in oil. Reweighing determines saturated weight. The core sample was pressured to 2,000 pounds per square inch before being placed in the core holder. To account for reservoir overburden pressure. The system was back-pressure-regulated. Back

strain was 1,000 pounds per square inch. Temperature and fluid injection matured the core for three days after changing pressure and temperature. Core sample had residual oil saturation after 24 hours of air injection. 24 hours after extended air infusion. Water and oil were collected in the test tube until the core sample stopped producing oil after injecting liquids.

Experiment with Alternating Fluid, Air and Oil Displacement

Only the final two manufacturers will inject fluids before air. As in the experiment, air, mixed fluid, and oil were conveyed. Add air or another ingredient after injecting liquid.

Flow Cell CFD Fluids Simulation

Introduction

CFD is the foundation of modern engineering analysis, allowing numerical study of fluid flow, turbulence, heat transfer, and multiphase transport under complicated situations [11]. By solving the Navier-Stokes equations of mass, momentum, and energy conservation, CFD allows engineers to predict behaviours that would be difficult, expensive, or prohibitive to test [12]. It is used in aircraft propulsion, medical systems, power production, petroleum recovery, and porous media research due to its versatility. Engineers use porous media in filters, catalytic reactors, geological formations, insulating systems, and oil recovery. Injection fluids interact with porous structures depending on permeability, porosity, and inertial resistance [13]. Alternative laws often represent the macroscopic pressure-velocity relationship. However, multiphase flow or successive injections complicate dynamics and make experimental observation insufficient [14]. CFD provides a systematic means to examine objects in a controlled environment. This study uses ANSYS Fluent to simulate three injection scenarios in a porous medium: fluid injection alone, air injection after fluid, and air injection after fluid. These examples show how adding phases in order impacts flow stability, energy loss, turbulence, and streamline redistribution. Results include pressure contours, velocity fields, streamline patterns, turbulence distribution, and residual convergence graphs. All these show how porous flow operates with distinct operational techniques.

5. Methodology

ANSYS Fluent followed the CFD workflow of pre-processing, solution, and post-processing (Figure 9). Each step is detailed below.

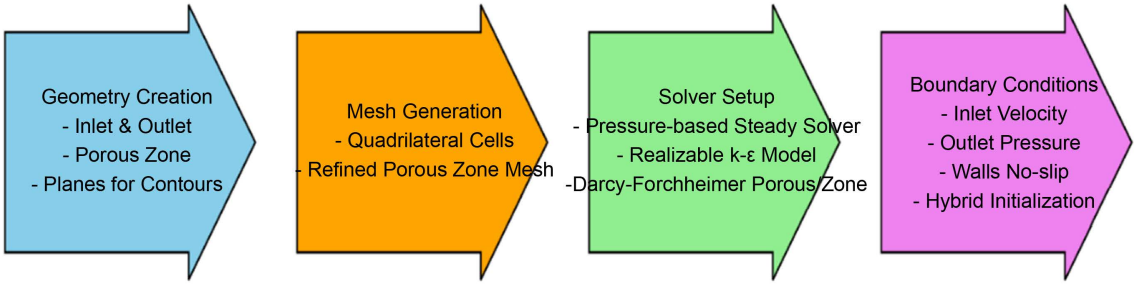

Figure 9. CFD workflow.

5.1. Geometry Creation

Creating computational geometry started the simulation. Simple 2D domain was used to illustrate porous medium setup. The geometry had an inlet, outlet, and porous zone. Additional planes were established across the domain to visualise pressure and velocity contours at different portions. The simplified 2D design maintained physical features while optimising computing.

5.2. Mesh Generation

Mesh discretised the domain after geometry was specified. Governing equations are solved in mesh cells. For 2D geometry, quadrilateral cells were chosen. A finer mesh was used in the porous region to capture gradients. Mesh quality is crucial: a coarse mesh risks numerical diffusion and inaccurate results, while a fine mesh increases computing effort. The mesh balanced precision and efficiency.

5.3. Solver Setup

The mathematical setup was carried out within ANSYS Fluent. A pressure-based steady-state solver was adopted with double precision enabled for mathematical accuracy. The key configurations were as follows:

- Turbulence model: Realizable k-ε model with scalable wall functions, suitable for general engineering flows.
- Porous zone: Represented using the Darcy-Forchheimer formulation with experimentally determined values of porosity and permeability.
- Gravity: Enabled to account for buoyancy-driven effects.
- Boundary conditions:
  - Inlet defined as a velocity/mass-flow inlet.
  - Outlet defined as a pressure outlet with backflow treatment enabled.
  - Walls treated as no-slip surfaces.
- Initialization: Hybrid initialization was applied to provide initial values for velocity, pressure, and turbulence quantities.

6. Results and Discussion

6.1. Ageing Core Sample

As time went on, crude oil-seasoned cores grew less watery. The core had a 17.2% oil recovery factor (RF) after three days in oil at 50˚C. For the core coated with brine after ageing, oil recovery was 11.5% RF (**Figures 10** and **Figure 11**). This was proven. Thus, the rock's wettability, which depends on its age, depends on brine and oil concentration and contact time. Ageing impacts rock; therefore, this seems correct. Age is modifying the sandstone; therefore, this is happening. This shows that crude oil adhesion to rock surfaces and wettability changes are reversible. During waterflooding, sandstone reservoirs should become wetter.

6.2. Porosity

A careful investigation and recording of dry core sample weights was done before

saturation. To ensure saturated core samples, this method was used. Wet core samples were weighed after saturation. Porosity of each core sample was calculated using Equation (3).

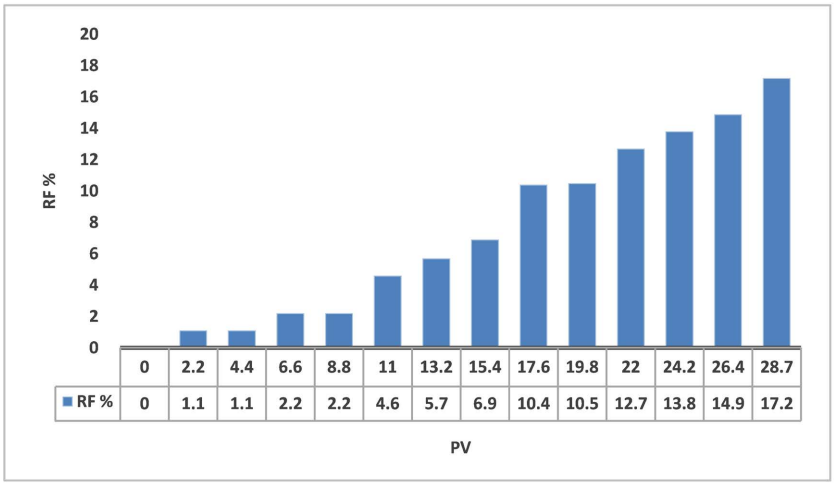

Figure 10. Oil recovery after ageing for three days.

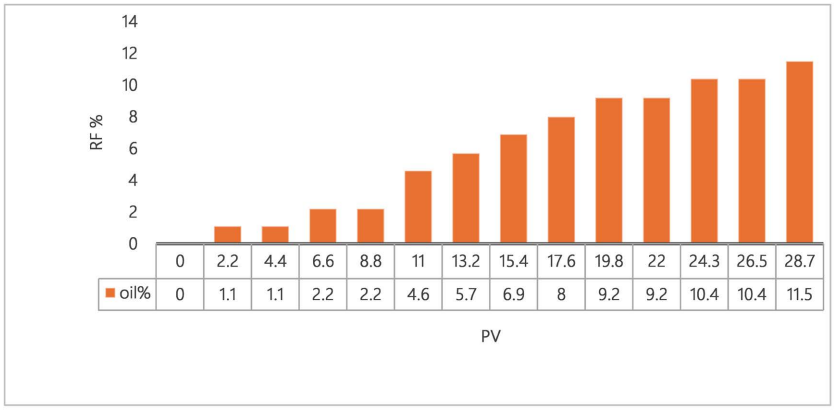

Figure 11. Oil recovery using zero-day ageing.

Using simple deductions, the following pore volumes of each core sample were measured and evaluated due to the collection 3:

$$\text{Pore Volume}\left(\text{PV}\right)=\frac{\text{Wet weight}-\text{Dry weight of sample}}{\text{Density of distted water}} \tag{3}$$

Distilled water has a density of 0.9982 grams per cubic centimetre. The results of the computations for the separate pore volumes produced by the core samples are shown in Table 3. It is possible to calculate the pore volumes by using the Equations (4) and (5) that are presented after this one.

$$\text{Volume}\left(\text{cm}^3\right)=\frac{\text{Mass}\ \left(\text{different wieght in g}\right)}{\text{Dinsity}\left(\frac{\text{g}}{\text{cm}^3}\right)} \tag{4}$$

As a further issue of interest, the porosity of every sample may be determined

by using the pore volumes, which are provided in Table 4.

Table 3. The amount of volume that was retrieved for each core sample.

Core samples	Weight different (g)	Bulk volume
Bentheimer	8.7	37.34
Castlegate	4.7	38.95
Leopard Sandstone	8	37.79
Salt Wash North	7.2	37.14
Michigan	7.3	39.55
Nugget	4	38.29

Table 4. The amount of porosity that was measured for each core sample.

Core samples	Weight different (g)	Bulk volume	Pore volume	Porosity %
Bentheimer	8.7	37.34	7.57	20.27
Castlegate	4.7	38.95	4.72	12.12
Leopard Sandstone	8	37.79	8.6	22.76
Salt Wash North	7.2	37.14	7.20	19.39
Michigan	7.3	39.55	7.32	18.51
Nugget	4	38.29	4	10.44

$$\text{Porosity} = \frac{\text{Pore Volume}}{\text{Bulk Volume}} \times 100 \tag{5}$$

6.3. Oil Recovery Factor

The lab-scale experiment uses enhanced oil recovery (EOR). A fluid removed oil from the core during the test, and production data was used to compute the oil recovery factor of these quantities 6.

$$\text{Recovery Factor}\,(\%) = \frac{\text{Production oil}}{\text{Original oil in place}} \times 100 \tag{6}$$

We calculated the amount of oil trapped inside the core and the overall volume of oil from the core flooding test using the saturated core sample we used for our research.

Research using silica nanoparticles with Arabic gum polymer: We tested fluid, air-fluid, and air-fluid combinations. Figure 12 shows that each scenario had a distinct experimental setting.

6.3.1. Scenario I (The Production of Oil Using Injection Fluid)

Injection fluids increase oil recovery by 15.7% - 16.7%. Silica nanoparticles improve oil recovery by reducing the water content of distilled water, Arabic gum polymer, and silica nanoparticle solutions from 32.34 to 18.66%.

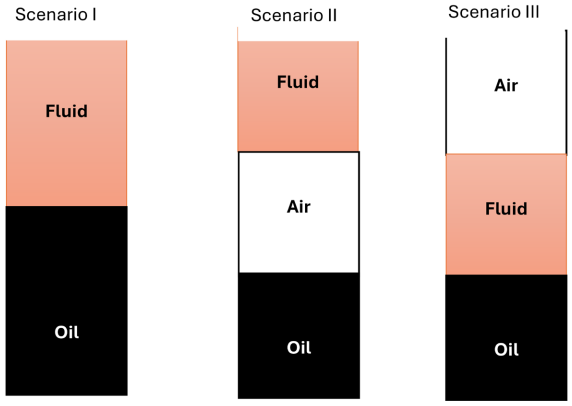

Figure 12. Structure of three different scenarios.

Bentheimer is a sandstone with 20.28% porosity and 1700 Md permeability

Core sample:	Sandstone (Bentheimer)
Porosity%:	20.28
Permeability:	1700 MD
Recovery factory%:	4
Water cut%:	21.3
Pore Volume injection:	32.4
Flow rate:	0.5 ml/m
Fluid used:	distilled water

After the oil was saturated and aged using distilled water, the injection was initiated at a flow rate of 0.5 millilitres per millimetre. (Figure 13 and Figure 14) Following the injection of 6.5 pore volumes (PV), oil production started, which led to a recovery of 1% for the oil and a reduction of 2.1% for the water cut. The oil recovery increased to 3.7% and the water reduction was 17.1% as soon as the PV injection hit 25.9. The oil recovery increased further, reaching 4.4% of its initial level after a cut reached 32.4%. According to the numbers below, any additional oil production vanished after the injection of 32.4 PV.

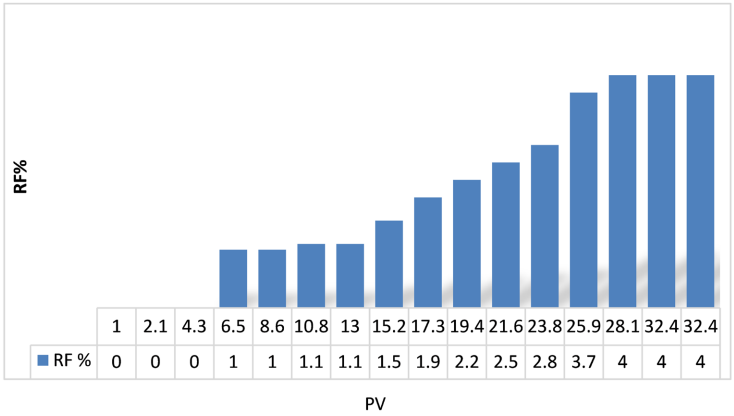

Figure 13. RF % of distilled water at various times.

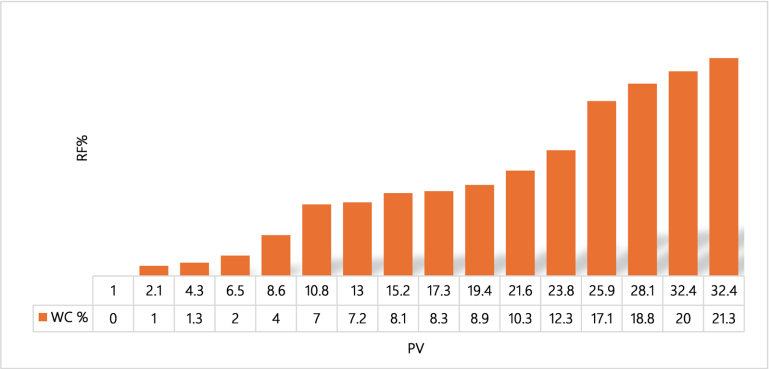

Figure 14. WC% of distilled water at various times.

6.3.2. Scenario II (Air Injection after Fluids to Produce Oil)

Combining injection fluid with air increases oil recovery by 11.5% to 20%. Silica nanoparticles in Arabic Gum polymer solutions reduced water content by 9% - 29%. This led to significant oil recovery. The reduction in polymer adsorption during silica-Arabic gum flooding may have improved sweep recovery factor and efficiency.

Sandstone Castlegate core sample has 1700 md permeability and 12.12% porosity

Core sample:	Sandstone (Castlgate)
Porosity%:	12.12
Permeability:	1700MD
Recovery factory%:	18.5
Water cut%:	9
Pore Volume injection:	28.7
Flow rate:	0.5 ml/m
Fluid used:	0.25wt. % silica nanoparticles, 0.25 wt.% polymer and 10 wt.% (brine)

Five weight percent brine was injected. An external vacuum operation at −1 bar for seven days saturated the core sample with oil. The core sample was then stored in a core holder at 50˚C for 24 hours. Brine injection began at 2.2 pore volumes (PV), resulting in 1.1% oil recovery and 0.5% water decrease. Oil recovery increased with brine injection, peaking at 28.7 PV, after which oil production stopped. After the floods, the recovery was 18.5% and the water cut was 9%. Please see Figure 15 and Figure 16 for more information.

6.3.3. Scenario III (Altering Air and Fluid to Produce Oil)

In the third injection, air was introduced first, followed by Arabic gum polymer and silica nanoparticles. This technique recovered the most oil with a recovery factor of 38.66% to 49.7% and a water cut of 1.07% to 12.7%. This technique as-

sumes that air will first fill the pore spaces, displace the oil, and increase its amount. This simplifies oil passage through the core sample route, increasing oil recovery.

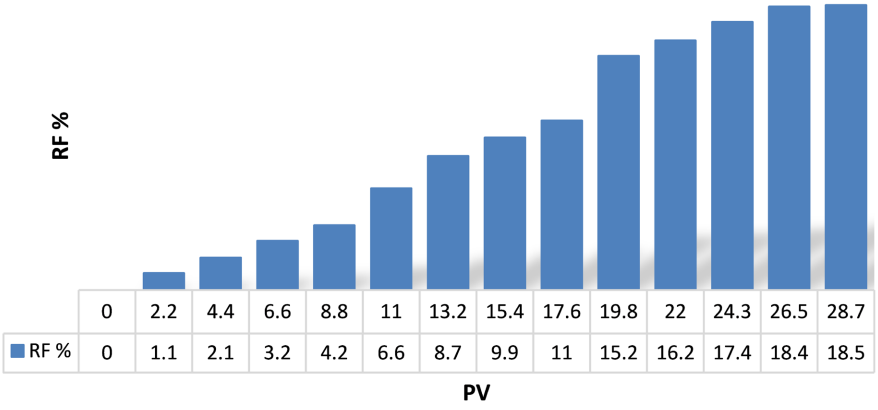

Figure 15. RF% of 0.5 wt.% silica nanoparticles and 0.25 wt.% polymer at various times.

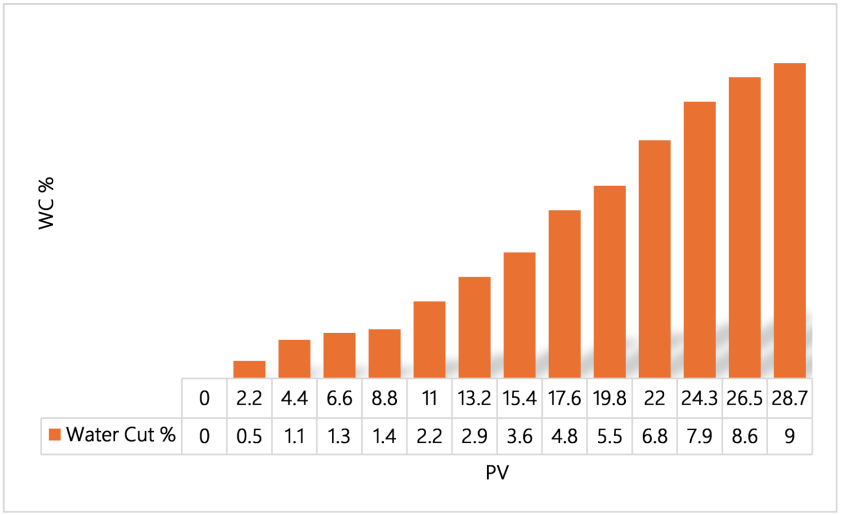

Figure 16. WC% at various times.

Sandstone family Leopard core sample with 900 mD permeability and 22.64% porosity

Core sample:	Sandstone (Castlegate)
Porosity%:	22.64
Permeability:	900MD
Recovery factory%:	48.6
Water cut%:	2.7
Pore Volume injection:	21.5
Flow rate:	1.25 ml/m
Fluid used:	0.3% polymer, 0.1% silica nanoparticles, and 5% brine.

After externally soaking the core sample in oil, it was carefully placed in the core holder and aged for 24 hours at 50 degrees Celsius. For twelve hours, the patient received air injections. Next, 0.1 weight percent silica nanoparticles and 0.3 weight percent Arabic gum polymer were injected at 1.25 millilitres per millimetre at 50 degrees Celsius. Injecting 5.8 PV of oil started production. When 10.5 PV was added, oil recovery increased 12.5%. After injecting 21.5 PV, air injection was continued for 12 hours, and then the alternate fluid was administered at the same flow rate. Oil production stopped after 21.5 PV injection. Following the flooding operation, 48.6% of the water was removed and 2.7% was reduced. See Figure 17 and Figure 18 for details.

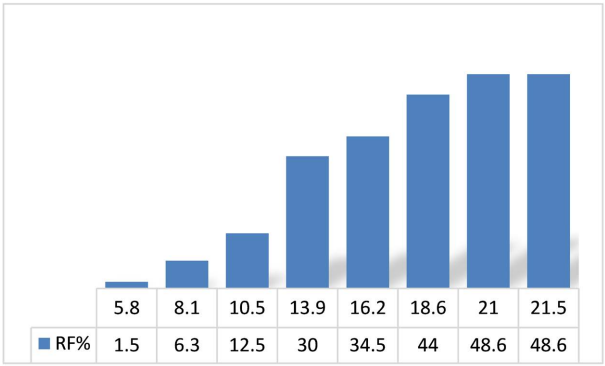

Figure 17. RF% for alternating air-water floods over time.

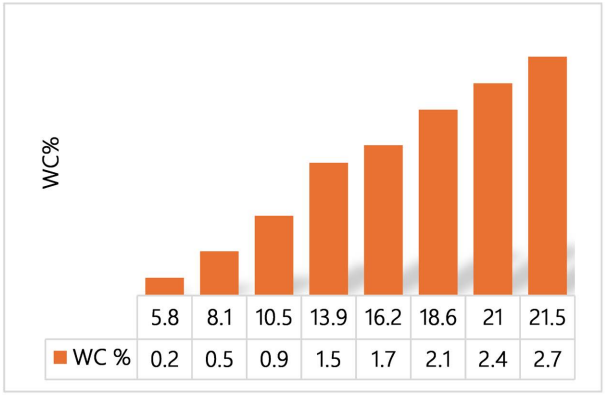

Figure 18. WC% volume relationship for alternating air-water floods over time.

6.4. Experimental Investigation of Three Scenarios

Figure 19 shows three scenarios' oil recovery results and outcomes. The image demonstrates that scenario three, AAW (air injection alternating with fluid), has the superior recovery factor compared to scenarios one and two. Calculating the recovery factor requires this link. Figure 19 demonstrates that the first scenario (fluid injection) and the second scenario (fluid alternative with air) had a higher water cut % than the first scenario. This happened in both cases. This is true based on the two situations. Very little crude oil was claimed due to the enormous in-

crease in water cut due to the breakthrough. At this point, several injection procedures add supercritical air into the system, lowering the water cut significantly. The percentage of water cut and oil recovery that has reduced is calculated using the following relationship:

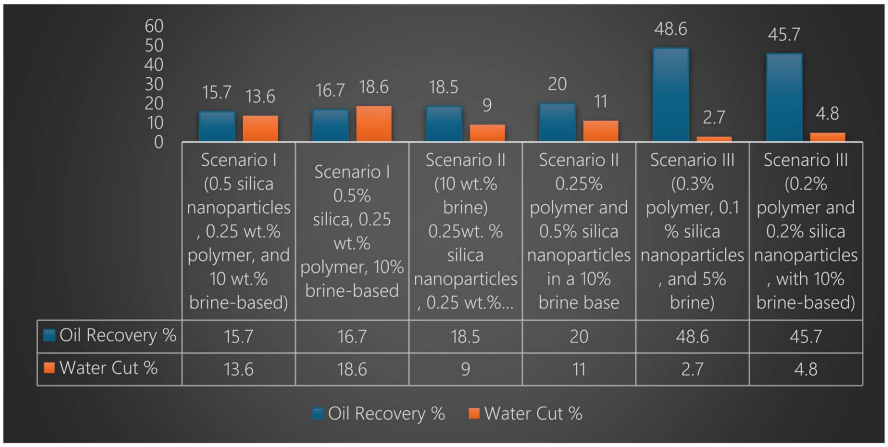

Figure 19. RF% and WC% in three different scenarios.

Figure 20 shows Scenario Three's oil recovery factor and water cut for air as an alternate fluid. This scenario uses water as a substitute fluid. In this case, air is an alternative fluid. The water cut chart and oil recovery factor for scenario three (air alterative fluid) and scenario two (fluid alterative air) are compared. Compare the two elements in the graphic below. This chart combines both charts. This study found that Scenario III will cut less water and extract more oil than Scenario II. The circumstance is different from scenario II, after considering scenario III.

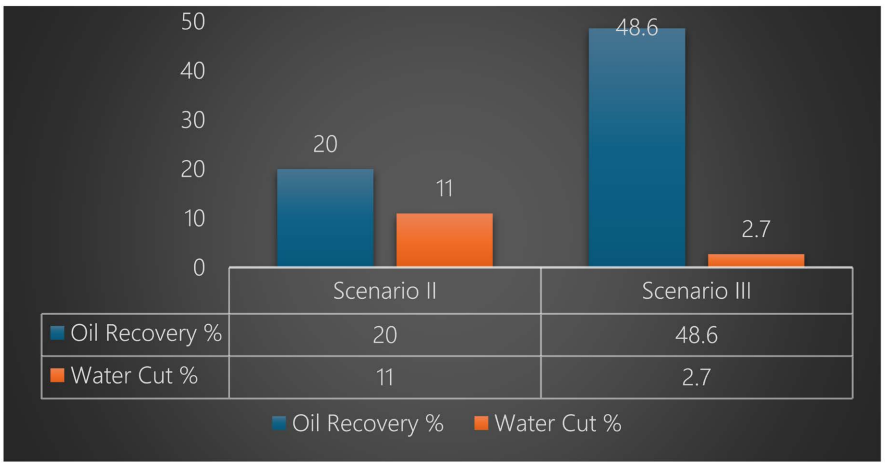

Figure 20. The reservoir at the same condition.

7. Flow Cell CFD Fluids Simulation

Simulation outputs included convergence histories, contour plots, and streamline visualisations. These outputs are detailed below.

7.1. Residual Convergence

Iterative solution residuals represent governing equation imbalance. Monitoring them is crucial for determining solution convergence. We tracked continuity, momentum (x, y), and turbulence characteristics (k and ε) in this experiment. The residual plot revealed consistent decreases in all variables, with most falling below 10^{-3}. The continuity residual stabilised around 10^{-4}, showing convergence. Porous flow simulations often result in a somewhat higher ε residual level. Overall, residual trend showed numerical stability.

7.2. Pressure Contours

From input to outflow, domain pressure contours were smooth. Inlet pressure was 597,000 Pa, exit pressure 573,000 Pa. This dip represents porous zone energy dissipation. The linear gradient supports Darcy's law, which predicts pressure decrease and velocity proportionality in porous media. Uniform distribution confirmed the porous formulation was implemented effectively.

7.3. Velocity Contours

Velocity distribution illuminated flow behaviour. In the core region of Plane 1, the greatest velocity was 3.61 m/s. Non-slip conditions reduced velocity near barriers. The porous medium's resistance reduced velocity in the porous zone. As expected, fluid accelerates in open channels but slows in porous resistance zones.

7.4. Streamline Visualization

Streamlines showed domain flow. The intake, porous region, and output all received uniform fluid. Some areas saw localised acceleration, peaking at 42 m/s. Recirculation pockets near porous surfaces indicate turbulence-porous interactions. The streamline patterns showed how the porous medium redirected flow and caused resistance.

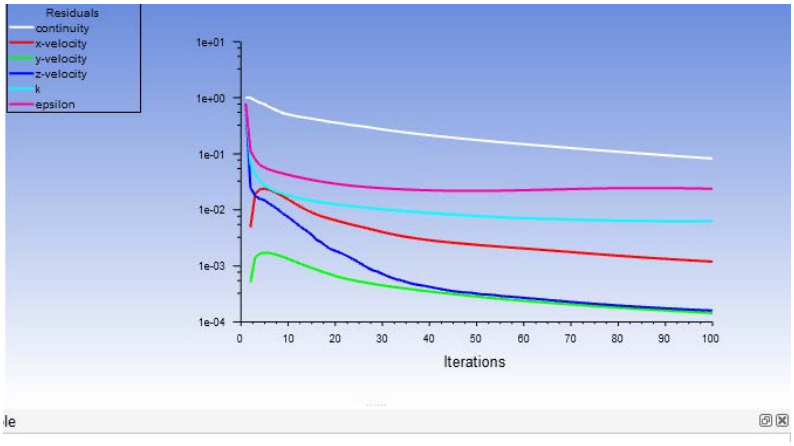

Figure 21. Residual convergence plot showing stable numerical behavior.

Figure 21 shows that continuity, velocity, and turbulence residuals are reduced

with iteration count, reducing error. Most residuals were below 10^{-3} and continuity dropped to 10^{-4}, indicating solver stability. The simulation's convergence dependability is confirmed by the continuous fall, which indicates decent mesh, boundary, and solver setup.

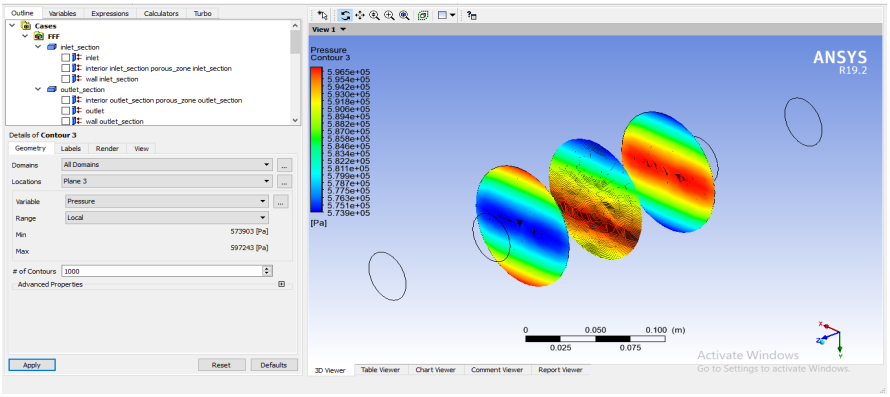

Figure 22. Pressure contour plot across the porous domain.

(Figure 22) Pressure contours show a smooth gradient from input to outflow, from 597,000 Pa to 573,000 Pa. The porous region loses pressure proportionally, following Darcy's law. The uniform gradient distribution confirms ANSYS Fluent's accurately implemented porous zone resistance model.

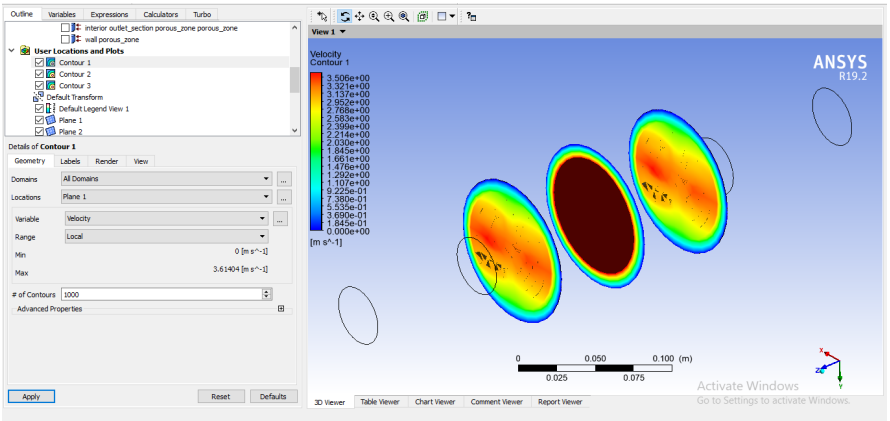

Figure 23. Velocity contours on Plane 1 highlighting velocity gradients.

The velocity contours show maximum flow intensity of 3.6 m/s in the central core and decreasing towards edges due to no-slip wall circumstances. Porous media increase resistance, lowering flow in afflicted places. These results confirm expected flow redistribution, showing core acceleration and damping from porous resistance in Figure 23.

The streamline visualisation in Figure 24 shows fluid entering uniformly at the intake, redistributing and accelerating via the porous zone, and departing at the outlet. Some channels had peak velocities approaching 42 m/s. Recirculation zones near porous surfaces indicate intricate internal redistribution mechanisms

due to turbulence-porous interactions.

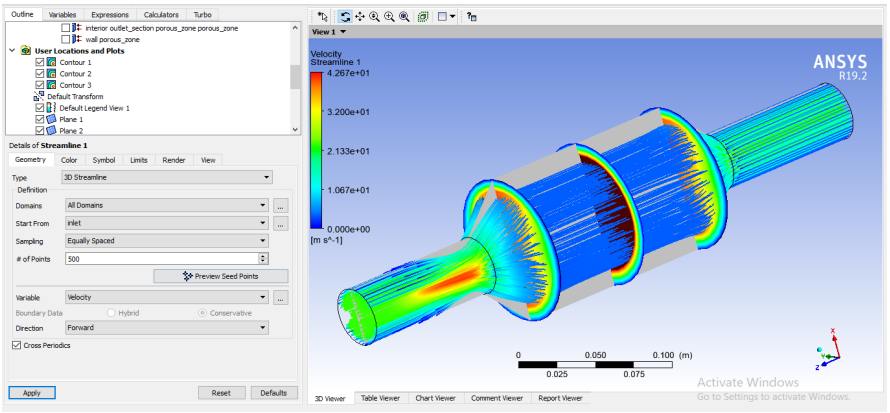

Figure 24. Streamlines showing redistribution of flow across the porous medium.

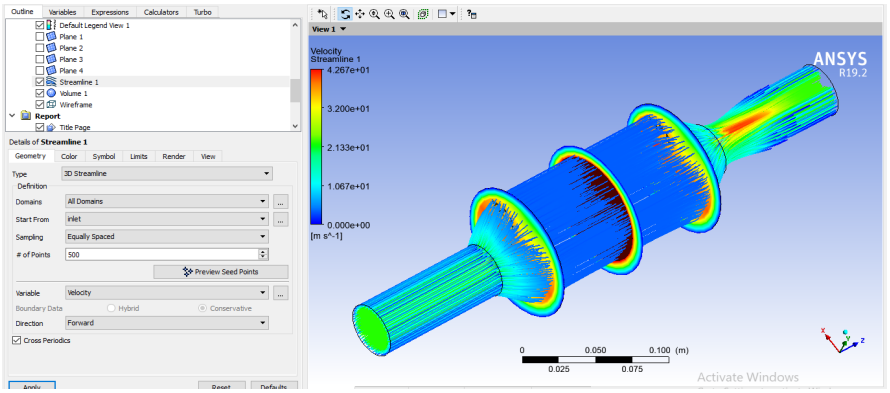

Figure 25. Streamlines with velocity magnitude indicating localized acceleration.

In Figure 25, streamline visualisation shows regions of amplified velocity with peak values of 42 m/s near confined porous sections. The colour map reveals strong core flow acceleration zones and sluggish fluid near walls due to boundary interactions. Turbulence-porous interactions and localised velocity amplification in the porous medium are confirmed by these patterns.

Evaluation of Scenarios

Comparisons of all three scenarios show differences in convergence behaviour, pressure distribution, velocity gradients, streamline features, and turbulence. Table 5 shows that injection sequence directly affects porous medium flow.

Comparing the three injection circumstances illuminates the intricacies of fluid and air movement in porous material. Different behaviours demonstrate the importance of injection sequencing in maintaining flow, turbulence, and energy dissipation. Residual convergence, pressure gradient, velocity fields, and streamline visualisations show that phase introduction sequence affects transport and mixing in porous structures.

8. Comparison of Scenarios

A comparative evaluation of all three scenarios shows the differences in conver-

gence behaviour, pressure distribution, velocity gradients, streamline characteristics, and turbulence levels. This comparison emphasises how the injection sequence directly influences porous media flow.

8.1. Scenario 1

Fluid injection into the porous medium was shown as the baseline. This example has the greatest domain-wide pressure drop, with entrance pressure reaching 2132.547446 Psi and output pressure 23.206038037 Psi. The porous zone's resistance caused the fluid to accelerate in localised areas over such a steep gradient. The velocity contours showed 41 m/s peaks, confirming this pattern. Streamline visualisation confirmed considerable jetting effects, with concentrated flow at the core and stationary zones along the walls. The temperature field remained steady at 49.850˚C, but mechanical energy dissipation was high. This scenario showed that injecting fluid alone is inefficient for porous medium applications due to high energy consumption and flow distribution instability.

Table 5. Comparison of scenarios.

Parameter	Scenario 1: Fluid Injection	Scenario 2: Air Injection Following Fluid	Scenario 3: Air is injected, and then fluid is injected
Residual Convergence	Stable; continuity ~1e−4, momentum ~1e−3.	Stable but slower; turbulence residuals are higher.	Stable; continuity ~1e−4, ε slightly higher.
Pressure Distribution	Inlet ~21320.55 psi → Outlet ~23.20603Psi.	Core pressure ~10863.32 Psi.	Inlet ~86.5875Psi → Outlet ~83.1066 Psi.
Velocity Distribution	Max ~41 m/s; jet-like acceleration.	Max ~24.5 m/s; smoother flow.	Max ~3.61 m/s; local acceleration up to ~42 m/s.
Streamline Behavior	Jet-like exit profile.	Smoother transitions; secondary circulation.	Uniform redistribution; recirculation near porous walls.
Temperature	~49.850˚C; nearly uniform.	~49.850˚C; minor variations.	Not explicitly shown; assumed uniform.
Overall Observation	Highest pressure drops, strongest jetting.	Balanced case with lower velocity peaks.	Most controlled flow; Darcy-like gradient.

8.2. Scenario 2

When air was added following fluid injection, behaviour changed dramatically. With core values about 10863.326556 Psi, the pressure field became more balanced, nearly half of Scenario 1. The porous zone's resistance decreased as air displaced portion of the fluid, as velocity contours exhibited lower peak values of 24.5 m/s. Streamlining visualisation showed smoother transitions, but multiphase interaction revealed additional circulations. The trade-off was that mixing between phases enhanced turbulence while reducing maximum velocity and pressure drop. This was corroborated by residual convergence, as turbulence residuals stabilised above Scenario 1. Despite this extra turbulence, Scenario 2 had a more regulated pressure distribution and less jetting, making it effective for avoiding velocity peaks.

8.3. Scenario 2

The most reliable and effective result. Pre-existing air pockets rerouted fluid flow. In contrast to the previous two situations, the input pressure was 86.587529425 Psi and the output pressure was 83.106623719 Psi, a much smaller but constant pressure drop. The velocity field averaged 3.61 m/s, with local acceleration zones exceeding 42 m/s. The streamline visualisations showed uniform redistribution with negligible recirculation. Darcy's law was closely obeyed, suggesting air dispersion stabilised the porous medium. This arrangement would use less energy and provide consistent, predictable flow, according to engineering.

9. Conclusion

Important implications can be derived from this investigation's facts. First, air injection and chemical flooding combined recover oil better than individually. Silica nanoparticles, Arabic gum, and air improve sweep efficiency and motion control, reducing channel oil. Second, the nano-polymer mixture's capacity to lower interfacial tension and change wettability allows this improvement. Lowering capillary forces that hold oil in rock pores allows the hybrid system to move and retrieve more oil. The overall conclusion is that reservoir conditions favour this method. Salinity, temperature, permeability, and porosity affect polymer and nanoparticle stability and recovery factor. Example: Sandstone cores with medium porosity and permeability recovered faster than dolomite cores with low permeability. Thus, reservoir testing is crucial before injection strategy selection. Fourth, the experiment reveals that air-injecting fluid injection balances mobility ratio, avoids breakthrough early, and produces longer than continuous injection. Finally, the results suggest that this hybrid method is technically solid and supports the industry's sustainability efforts. Arabic gum makes EOR cheaper and greener than synthetic polymers. The CFD simulation showed that injection order affects porous material flow efficiency. Fluid injection caused pressure loss and jetting. Adding air after the fluid helped it flow more easily, but more turbulently. Giving fluid made flow the most stable and energy-efficient after air, with consistent pressure distribution and the same speed profiles. Air preconditioning stabilises flow and saves energy. This is the best way to infuse porous systems.

Conflicts of Interest

The authors declare no conflicts of interest regarding the publication of this paper.

References

[1] Guo, S., Wang, H., Shi, J., Pan, B. and Cheng, Y. (2014) Synthesis and Properties of a Novel Alkyl-Hydroxyl-Sulfobetaine Zwitterionic Surfactant for Enhanced Oil Recovery. *Journal of Petroleum Exploration and Production Technology*, **5**, 321-326. https://doi.org/10.1007/s13202-014-0141-y

[2] Zhang, J., Gu, M., Zheng, T. and Zhu, J. (2009) Synthesis of Gelatin-Stabilized Gold Nanoparticles and Assembly of Carboxylic Single-Walled Carbon Nanotubes/Au Composites for Cytosensing and Drug Uptake. *Analytical Chemistry*, **81**, 6641-6648.

https://doi.org/10.1021/ac900628y

[3] Ting, B.P., Zhang, J., Gao, Z. and Ying, J.Y. (2009) A DNA Biosensor Based on the Detection of Doxorubicin-Conjugated Ag Nanoparticle Labels Using Solid-State Voltammetry. *Biosensors and Bioelectronics*, **25**, 282-287. https://doi.org/10.1016/j.bios.2009.07.005

[4] Kumar, A. and Dhawan, A. (2013) Genotoxic and Carcinogenic Potential of Engineered Nanoparticles: An Update. *Archives of Toxicology*, **87**, 1883-1900. https://doi.org/10.1007/s00204-013-1128-z

[5] Babadagli, T. (2020) Philosophy of EOR. *SPE/IATMI Asia Pacific Oil & Gas Conference and Exhibition*, Bali, 29-31 October 2019, SPE-196362-MS. https://doi.org/10.2118/196362-ms

[6] Lee, S., Choi, S.U., Li, S. and Eastman, J.A. (1999) Measuring Thermal Conductivity of Fluids Containing Oxide Nanoparticles. *Journal of Heat Transfer*, **121**, 280-289. https://doi.org/10.1115/1.2825978

[7] Wasan, D.T. and Nikolov, A.D. (2003) Spreading of Nanofluids on Solids. *Nature*, **423**, 156-159. https://doi.org/10.1038/nature01591

[8] Amott, E. (1959) Observations Relating to the Wettability of Porous Rock. *Transactions of the AIME*, **216**, 156-162. https://doi.org/10.2118/1167-g

[9] Anderson, W. (1986) Wettability Literature Survey—Part 2: Wettability Measurement. *Journal of Petroleum Technology*, **38**, 1246-1262. https://doi.org/10.2118/13933-pa

[10] Vurro, M., Miguel-Rojas, C. and Pérez-de-Luque, A. (2019) Safe Nanotechnologies for Increasing the Effectiveness of Environmentally Friendly Natural Agrochemicals. *Pest Management Science*, **75**, 2403-2412. https://doi.org/10.1002/ps.5348

[11] Bhatti, M.M., Marin, M., Zeeshan, A. and Abdelsalam, S.I. (2020) Editorial: Recent Trends in Computational Fluid Dynamics. *Frontiers in Physics*, **8**, Article 593111. https://doi.org/10.3389/fphy.2020.593111

[12] Zikanov, O. (2019) Essential Computational Fluid Dynamics. John Wiley & Sons.

[13] Ranjbarzadeh, R. and Sappa, G. (2025) Numerical and Experimental Study of Fluid Flow and Heat Transfer in Porous Media: A Review Article. *Energies*, **18**, Article 976. https://doi.org/10.3390/en18040976

[14] Govindarajan, S.K. (2019) An Overview on Extension and Limitations of Macroscopic Darcy's Law for a Single and Multi-Phase Fluid Flow through a Porous Medium. *International Journal of Mining Science*, **5**, 1-21.